Basal forebrain control of prefrontal cortical function during fear learning
Final report of OTKA-PD 116347 project

The mechanism of associative learning is a highly investigated topic since the introduction of optogenetic and chemogenetic tools and the fast evolution of gene manipulation techniques. These two methods provide accessibility to selective switching on and off neural functions in a cell-type specific manner, which allow deep insights to uncover the operational mechanisms of neural circuits underlying behaviour paradigms such as fear conditioning. The two main cortical areas involved in this aversive type of associative learning are the prefrontal cortex and basolateral amygdala. Although our knowledge about neural processes forming fearful memories has substantially expanded, the pathway responsible for delivery of aversive stimuli is still obscure. Based on previous data we hypothesized that the basal forebrain may be a good candidate for transferring aversive information to cortical regions as this subcortical region has been previously shown to affect fear related memory formation (Craig et al., 2009, Tronson et al., 2009, Kaifosh et al., 2013, Jiang et. al., 2016), and known to be activated to unanticipated stimuli (Hangya et.al., 2015).

In my OTKA-PD project we aimed to investigate the effect of the basal forebrain (BF) GABAergic projection in an aversive learning paradigm, fear conditioning in which the prefrontal cortex (PFC) was involved (Courtin et al., 2013). To achieve this, first we planned to anatomically map the projections of the several subdivisions and cell types of BF to distinct PFC areas using neural tracing and immunohistochemistry, and with *in vitro* electrophysiological experiments to test for functionality. Then, we wished to investigate the relevance of this pathway with *in vivo* behaviour essays.

As the basal forebrain is a complex structure consisting of several areas, first we investigated which subdivisions project to the prefrontal cortex. As the different parts of the PFC can be responsible for opposite functions such as fear acquisition or extinction, we targeted the prefrontal cortical subdivisions selectively and distinctively. Therefore, we performed retrograde tracing with fluorogold (FG) injected to three prefrontal cortical regions: prelimbic cortex (PL), infralimbic cortex (IL), and anterior cingulate cortex (ACC). From the ACC, we found a sparse number of retrogradely labeled cells in the BF. Cells projecting to the PL or IL were not segregated in the BF, they were both localized in the ventral pallidum (VP), substantia innominata (SI), magnocellular preopticus nucleus (MCPO) and horizontal diagonal band (HDB). As comparison, we also labeled basal amygdala (BA) with fluorogold to test for BF projection cells to another region involved in fear learning (Pape and Paré, 2010, Duvarci and Paré, 2014). We found that BA-projecting BF cells were predominantly localized in the VP/SI and in smaller number in the MCPO and HDB (Figure 1).
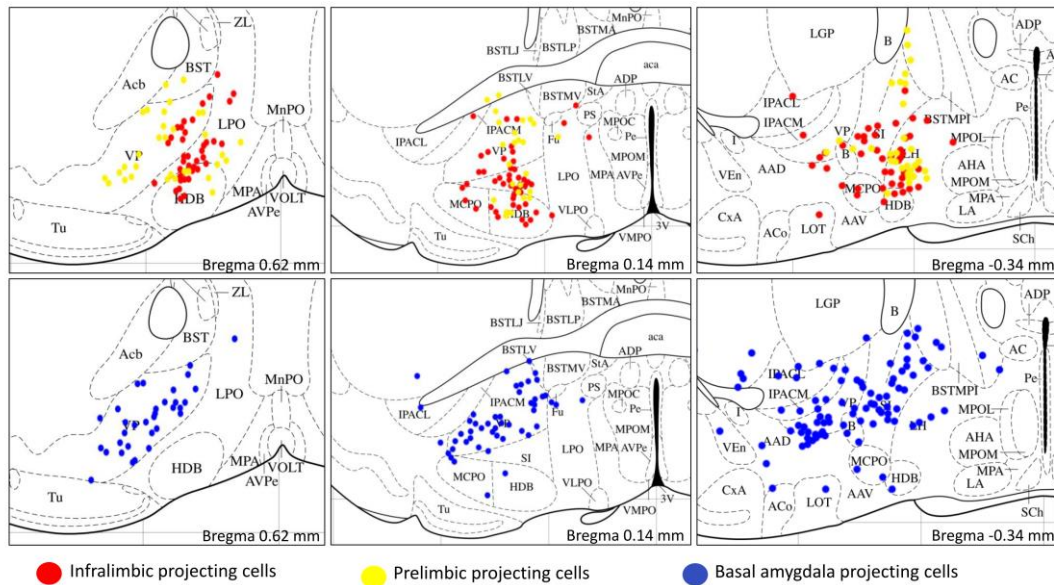
Figure 1. Localization of cells in the basal forebrain projecting to the infralimbic cotex (IL), prelimbic cortex (PL) and basal amygdala (BA). Localization maps were reconstructed in three planes. Data are obtained from retrograde tracing experiments, where fluorogold was injected to the IL, PL and BA, respectively. Injection coordinates: PL: AP: 1.9 mm, ML: 0.3 mm, DV: 1-1.5 mm; IL: AP: 1.9 mm, ML: 0.3 mm, DV: 1.9-2.2 m; BA: AP: 1.5 mm, ML: 3-3.2 mm, DV: 4.2-4.4 mm)

To determine the GABAergic proportion of PFC projecting BF cells, we immunostained PV on the labeled samples. Surprisingly, we found very few FG-positive, i.e. retrogradely labeled cells in the BF that showed PV immunoreactivity (below 5%). As a further attempt to estimate the number of GABAergic projection cells, we repeated the retrograde tracing in VGAT reporter mice (vGAT-cre X Gt(rosa)26Sor_CAG/LSL_ZsGreen1), where the GABA-containing cells express green fluorescent protein. In these experiments, we found that roughly 90% of projecting cells are GABAergic. In parallel, we also stained choline acetyltranferase (CHAT) on retrogradely labeled cells to examine the ratio of cholinergic projection. In these experiments, we found that almost all cholinergic cells co-express GABA, which hasn't been shown before in the BF. To confirm this result, we selectively injected VGAT-Cre mice with a Cre-dependent AAV viral vector (AAV2/8-Flex-GFP) to the VP/SI or HDB to anterogradely label the PL/IL projecting cells and verify the presence of axonal projection. Intriguingly, in these experiments, we failed to find profound GABAergic projection to the PFC areas. The axons from both areas rather targeted the medial orbital cortex (MO), deep layers of IL and secondary motor cortex (M2). In the same time, when we stained CHAT on GFP-labeled cells in the BF, we observed a negligible overlap between putative GABAergic and cholinergic cells (Figure 2). These results may suggest that during early development VGAT is expressed in many BF neurons, which expression changes with time and in adult mice VGAT and CHAT show only a minor overlap. In spite of the fact that in adult mice VGAT and CHAT projection to the PFC can be separately studied, we found that the GABAergic projection from the BF to the PFC is not strong enough to perform functional *in vitro* or *in vivo* experiments. Therefore, we decided to investigate the relationship of the BF and PFC from other aspects.
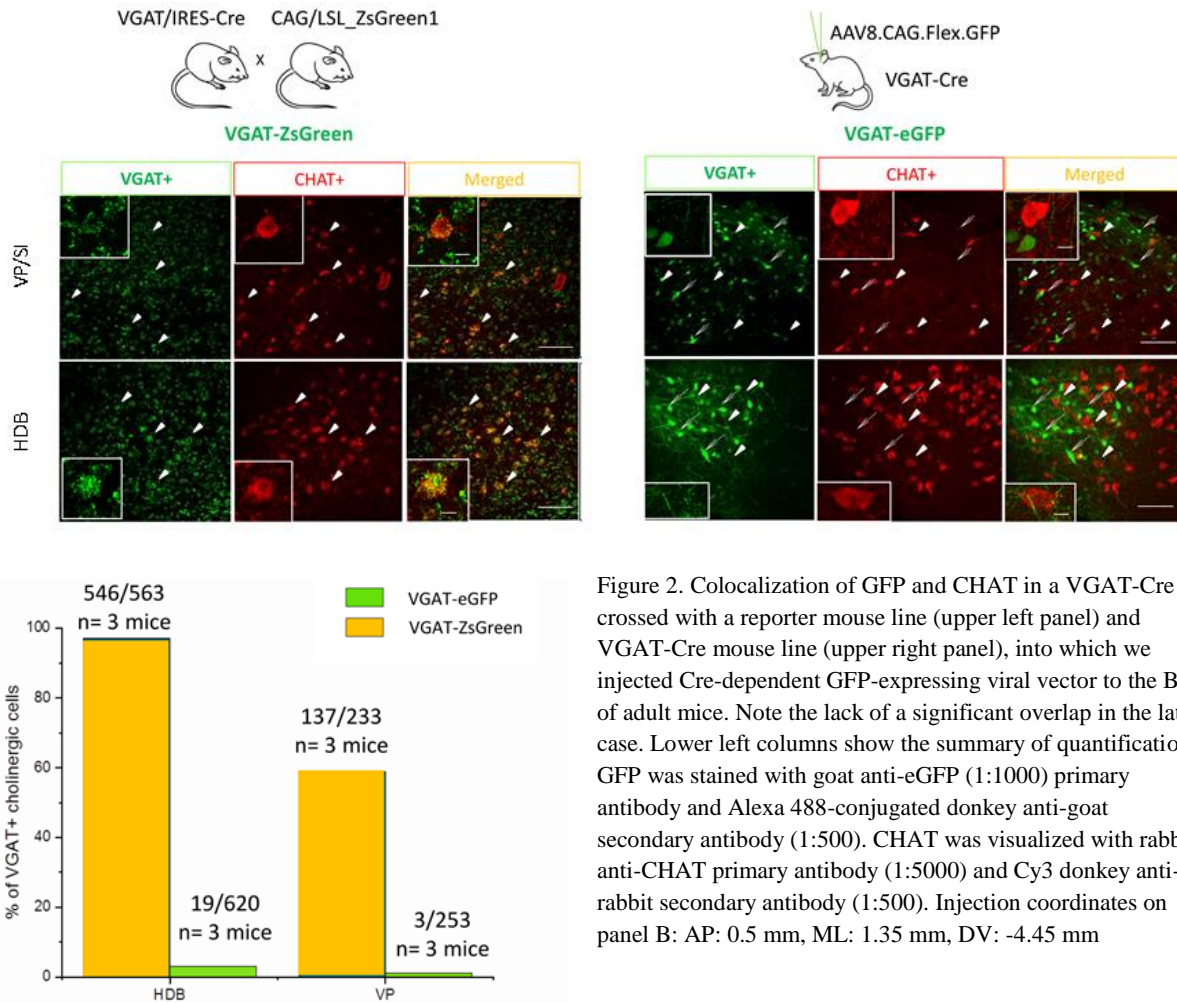
Figure 2. Colocalization of GFP and CHAT in a VGAT-Cre crossed with a reporter mouse line (upper left panel) and VGAT-Cre mouse line (upper right panel), into which we injected Cre-dependent GFP-expressing viral vector to the BF of adult mice. Note the lack of a significant overlap in the latter case. Lower left columns show the summary of quantification. GFP was stained with goat anti-eGFP (1:1000) primary antibody and Alexa 488-conjugated donkey anti-goat secondary antibody (1:500). CHAT was visualized with rabbit anti-CHAT primary antibody (1:5000) and Cy3 donkey anti-rabbit secondary antibody (1:500). Injection coordinates on panel B: AP: 0.5 mm, ML: 1.35 mm, DV: -4.45 mm

In contrast to the intermingled cell populations projecting from the BF to the PL and IL, we found that the projecting cells from the basal amygdala (BA) to the different PFC regions show a marked topology. PL-projecting cells cumulate in the anterior part of the BA (aBA), while the number of the IL-projecting cells are higher in number in the posterior parts (pBA) (Figure 3). These results are contrary to what was reported in Senn et al., 2014 but support the findings of Kim et. al., 2016.
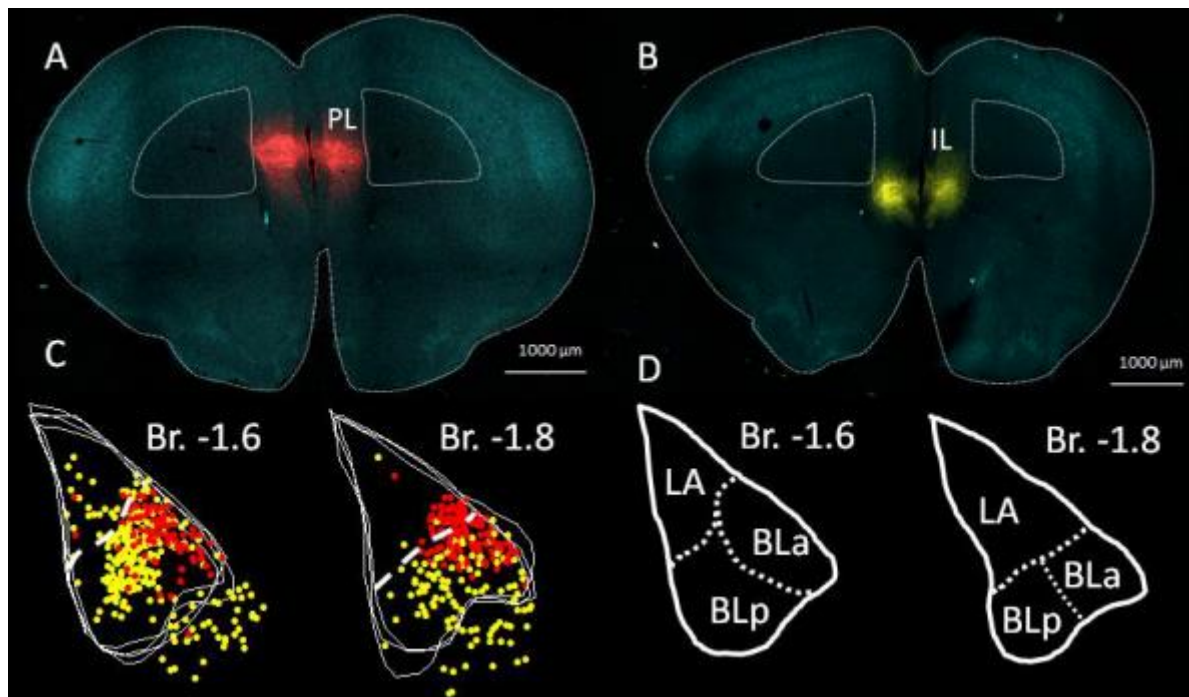
Figure 3. Mapping amygdalar cells projecting to the PL (red) or IL (yellow) in panel C in two planes (D) obtained by retrograde tracing with fluorogold. Panel A and B demonstrate the site of bilateral injections. N=2 for PL and IL, respectively.

We confirmed the segregation of PL and IL projecting cells in the BA by double retrograde staining of PL and IL projecting BA neurons with injection of two different tracers (fluorogold and fast blue). To further examine the BF projection, we injected retrograde tracer fast blue to the BA and in the same time fluorogold to PL or IL to check whether there are double-projecting cells at the level of BF. As a result, we found only a few BF cells that projected to both regions (less than 5%), although the localization of the BA projecting cells overlapped with the PL/IL projecting cells at the level of the VP/SI. These results were presented at the FENS regional meeting in 2017 held in Pécs titled "Structural basis for the basal forebrain control of the medial prefrontal cortex and basal amygdala".

We characterized the ratio of the cholinergic projection cells in the BF to PFC and BA using CHAT immunohistochemistry. We found that 61% of BA projecting cells are CHAT+, while only 24% and 27% of PL- and IL projecting cells were CHAT+, respectively.

To describe the localization of the projecting axons in the BA and PFC regions, we injected AAV viral vector to CHAT-Cre mice selectively to VP/SI and HDB and compared the projection of these two areas. Interestingly, at the BLA level, we found marked differences in cholinergic innervation originated from the VP/SI and HDB. VP/SI cholinergic axons almost exclusively targeted the BA (almost 80% of axons could be found within the BA), whereas the projection from the HDB to the BLA was more diffuse, but avoiding the BA (less than 10 % of axons could be found there) and targeting the surrounding regions, including the anterior and posterior parts of basomedial amygdala, posteromedial cortical amygdaloid nucleus, piriform cortex, lateral entorhinal cortex (Figure 4).

AAV8.CAG.Flex.GFP injected into Chat-Cre mice

Injection site

Bregma 0.4 mm

ac

HDB

VP

500 µm

Bregma 0.1 mm

ac

HDB

VP/SI

Target site

LA

BA

500 µm

LA

BMA

BA

BAP

Merged data

Bregma -1.3 mm

LA

Den

CeM

BA

MeA

BMA

Pir

ACo

Bregma -1.9 mm

LA

DEn

MeP

BA

BMP

Pir

PMC

Bregma -2.7 mm

DEn

BMP

Ahi

LEnt

PMC

Apir

━━ Mouse 1   ━━ Mouse 2   ━━ Mouse 3
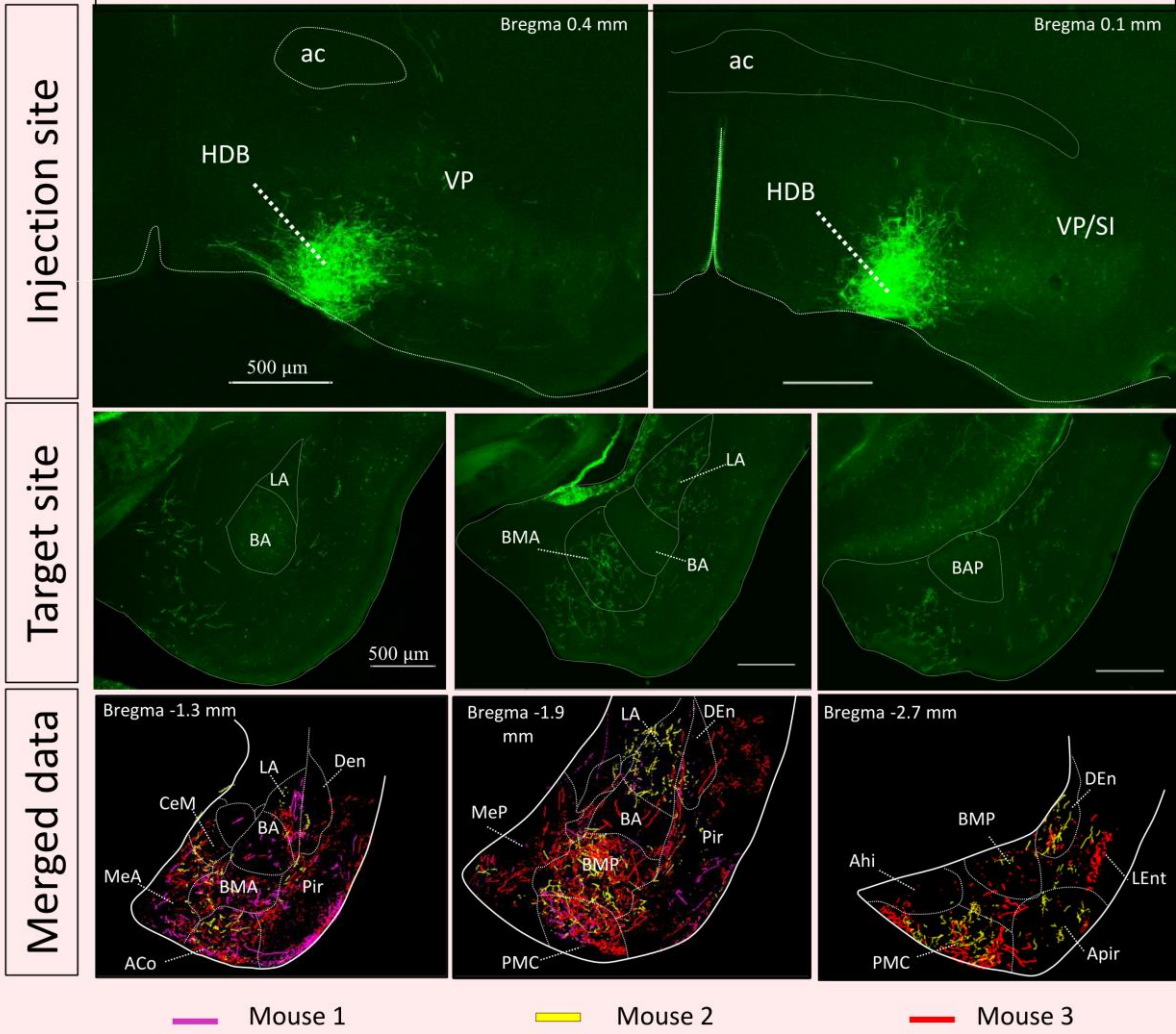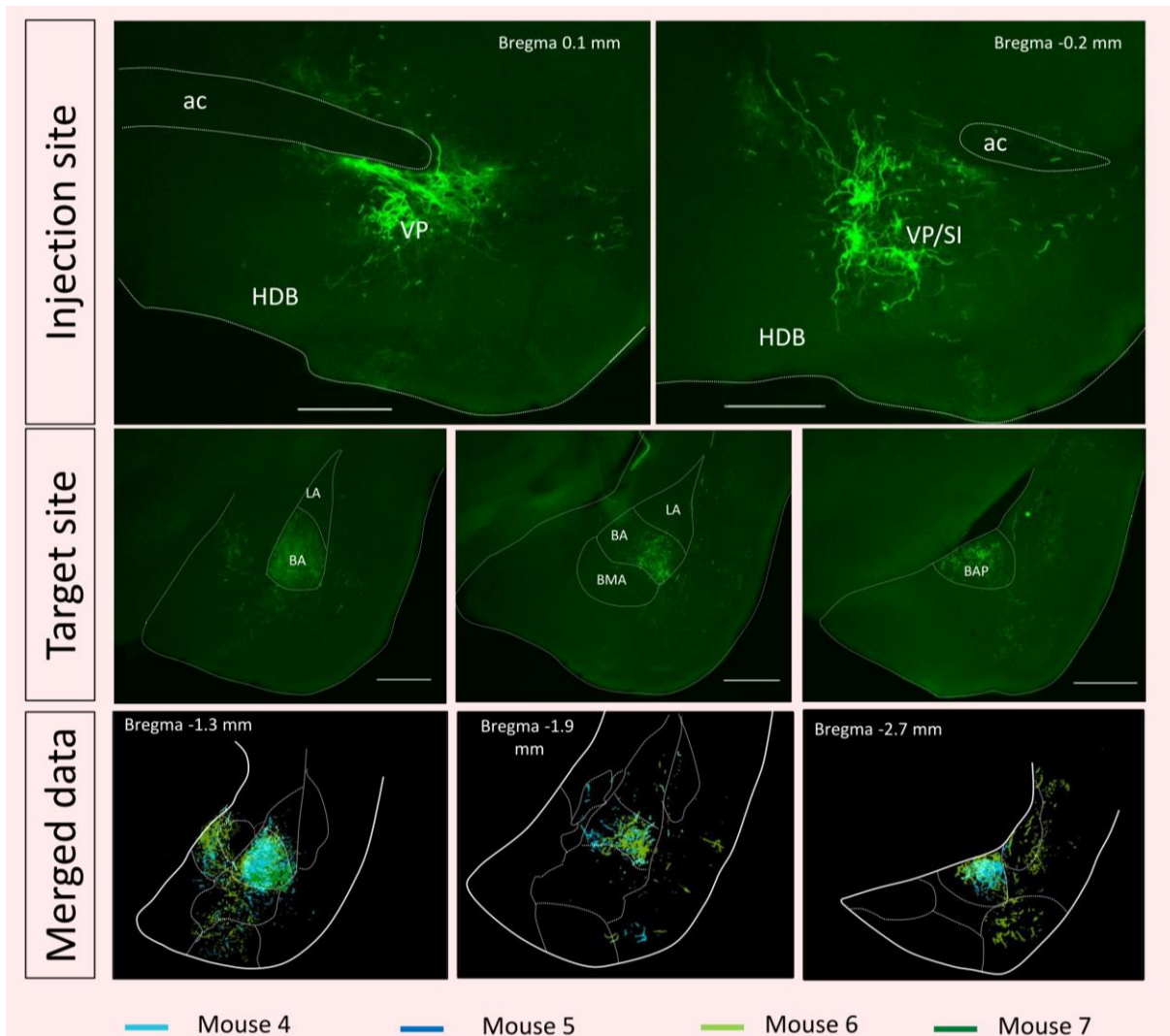
Figure 4. Cholinergic innervation of the amygdala region by the two basal forebrain areas, VP/SI and HDB is complementary. Representative images of injection sites to the HDB (upper panel) or VP/SI (lower panel) in the upper row of the panels, and axonal projections in the amygdala region in the middle row of the panels from the HDB (upper panel) or VP/SI (lower panel), respectively on three coronal planes. Lower row of panels: merged data from reconstruction of 3 and 4 experiments, respectively. Injection sites were as follows. HDB: AP/ML/DV, 0.5/0.7/5.0 m, VP/SI (AP/L/DV, 0.5/1.5/4.4 mm) in CHAT-cre mice. ac, anterior commissure; ACo, anterior cortical amygdaloid nucleus; Ahi, amigdalohippocampal area;Apir, amigdalopiriform transition area;BA, basal amygdaloid nucleus; BAP, basal amygdaloid nucleus , posterior part; BMA, basomedial amygdaloid nucleus, anterior part; BMP, basomedial amygdaloid nucleus, posterior part; CeM, central amygdaloid nucleus,medial division; DEn, dorsal endopiriform nucleus; HDB, nucleus of the horizontal limb of the diagonal band; LA, lateral amygdaloid nucleus; LEnt, lateral enthorinal cortex; MeA, medial amygdaloid nucleus, anterior part; MeP, medial amygdaloid nucleus, posterior part; Pir, piriform cortex; PMC, posteromedial cortical amygdaloid nucleus; SI, substantia innominata;VP, ventral pallidum
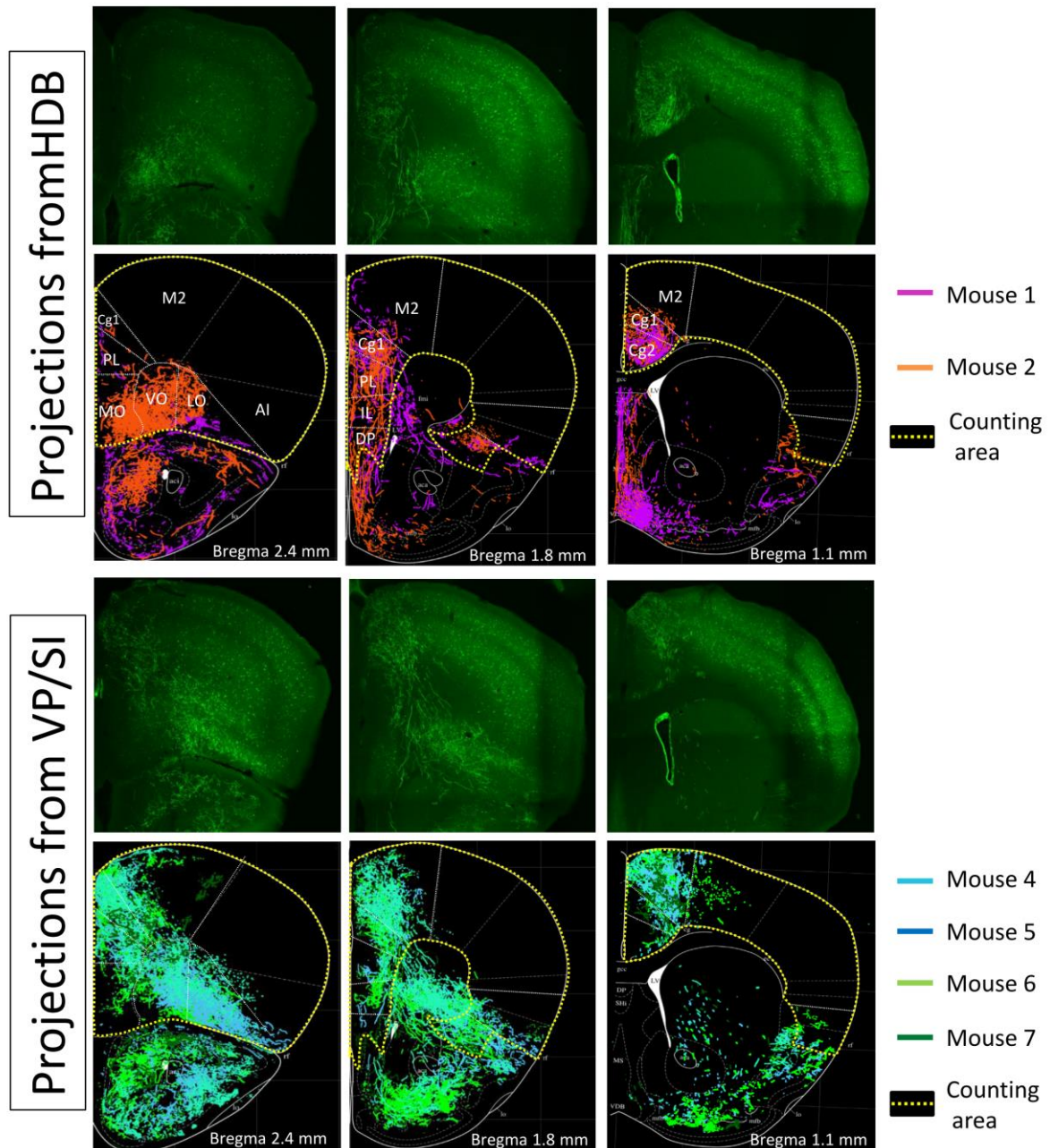
Figure 5. Cholinergic axonal projection from the HDB and VP/SI overlaps in the mPFC. Representative images and reconstruction of 3 and 4 experiments respectively, on three coronal planes of the projection of HDB or VP/SI to prefrontal cortical regions. AI, agranular insular cortex; Cg1, cingulate cortex, area 1; Cg2, cingulate cortex, area 2; DP, dorsal peduncular cortex; IL, infralimbic cortex; LO, lateral orbital cortex; M1, primary motor cortex; M2, secondary motor cortex; MO, medial orbital cortex; PL, prelimbic cortex; VO, ventral orbital cortex

In contrast, when we examined the sections containing the mPFC, we observed that the cholinergic projection from the VP/SI and HDB showed a marked overlap. Both areas projected to the ventral and lateral orbital cortex, cingulate cortex area 1, IL, PL, agranular insular cortex in a similar manner. However, VP/SI projected more profoundly to M2, while HDB had selectivity to cingulate cortex (Figure 5). We constructed maps of the cholinergic

projections from these two BF regions obtained in 3-3 mice. These results were presented at the FENS 2018 meeting held in Berlin, titled: "Amygdala region is innervated by two distinct groups of cholinergic cells located in the basal forebrain".

Concerning the cholinergic innervation of basal amygdala, we have started to investigate its impact on local circuitry using *in vitro* electrophysiology. We injected AAV carrying DIO-ChR2-eYFP construct to the BF of CHAT-Cre, or VGLUT3-Cre mice (this latter was also known to send cholinergic axons to BA (Poulin et al., 2006)), and we studied the light-evoked postsynaptic currents (PSCs) in BA cells that were *post hoc* identified based on morphology and firing pattern. During recordings, we applied nicotinic and muscarinic acetylcholine receptor (AchR) antagonists to test for the receptors responsible for the effects of the released neurotransmitter molecules. After analysis of the recordings, we found that distinct cell types were affected differently by BF cholinergic inputs. Principal cells displayed muscarinic acetylcholine receptor (mAchR)-dependent (i.e. atropine-sensitive) slow outward responses (10/18 cells). In cholecystokinin (CCK)+ basket cells, we recorded either outward (14/33) or inward (11/33) PSCs: the former responses could be blocked by atropine, while the latter were sensitive to nicotinic acetylcholine receptor (nAchR) antagonists dihydro-b-erythroidine hydrobromid (DHßE) and methyllycaconitine (MLA). In vasoactive intestinal polypeptide (VIP)+ and neurogliaform cells (NGFCs), we found DHßE- and MLA-sensitive currents (VIP+: 12/14, NGFCs: 5/5 cells). Axoaxonic cells (AACs) exhibited large currents evoked by cholinergic fiber stimulation (we detected responses in 29 out of 33 AACs) that could be abolished only by the wide spectrum nAchR antagonist hexamethonmium, in a relatively large concentration (1 mM, tested on 13 cells). In PV+ basket cells we rarely observed small inward currents upon ChR2 stimulation (2/16 cells) (Figure 6). A part of these *in vitro* results was presented at the MITT 2019 conference held in Debrecen titled "Noxious stimulation excites both principal neurons and interneurons in the basolateral amygdala complex *in vivo*".

PC

20 mV
200 ms

↓↓↓↓↓   ctr
         atropine   20 pA
                     100 ms

AAC

20 mV
200 ms

↓   ↓   ↓   ↓   ↓

ctr
1 mM hexamethonium

20 pA
100 ms

PV BC

20 mV
200 ms

↓   ↓   ↓   ↓   ↓   20 pA
                     100 ms

NGF

20 pA
200 ms

↓   ↓   ↓   ↓   ↓

10 pA
100 ms

ctr
dhbe mla

20 um

CCK BC

20 mV
200 ms

ctr
atropine

20 pA
100 ms

20 mV
200 ms

20 pA
100 ms

ctr
5 uM DHBE+MLA

VIP

20 mV
200 ms

20 pA
100 ms

ctr
5 uM DHBE+MLA
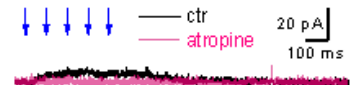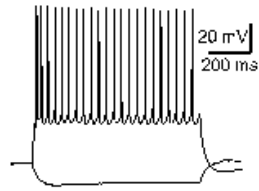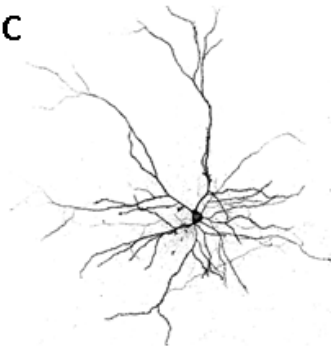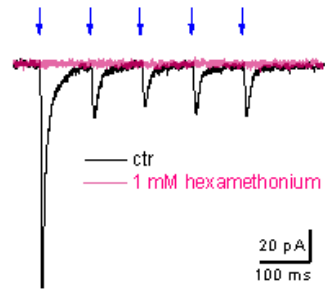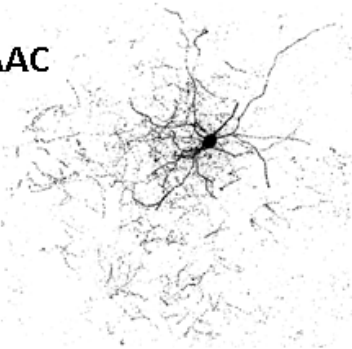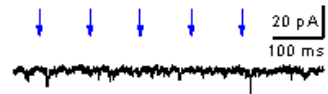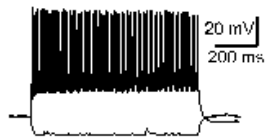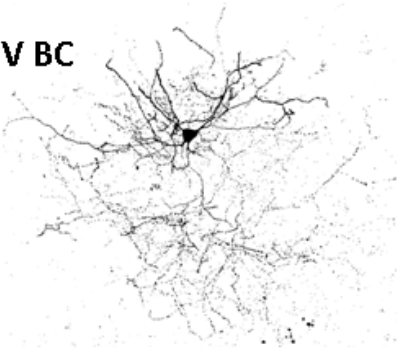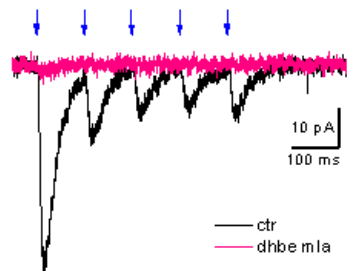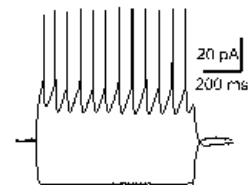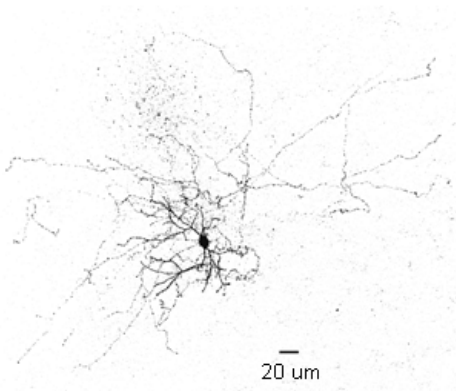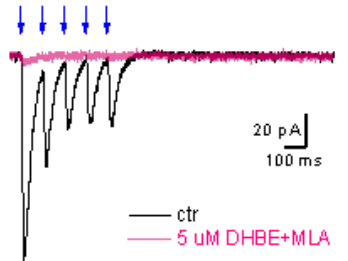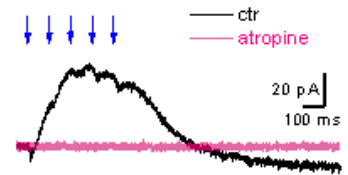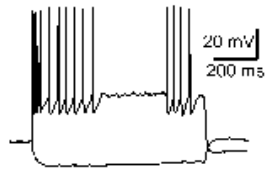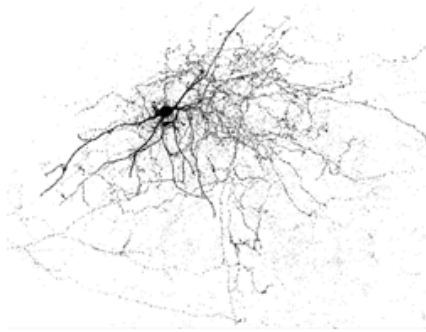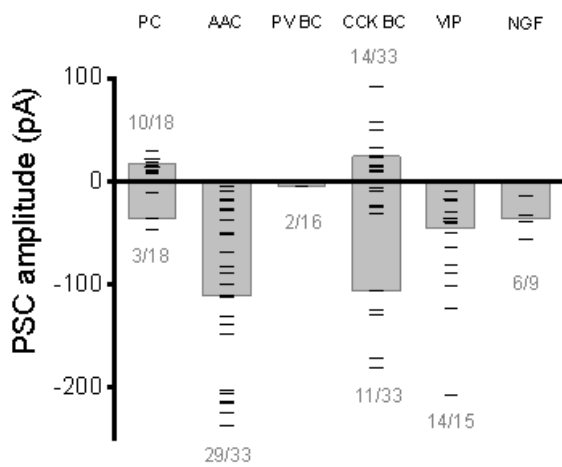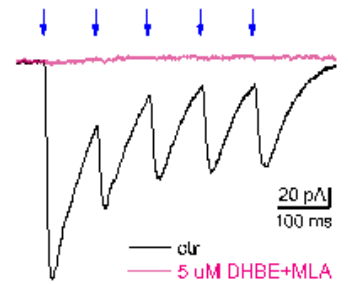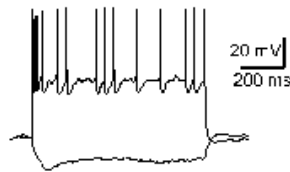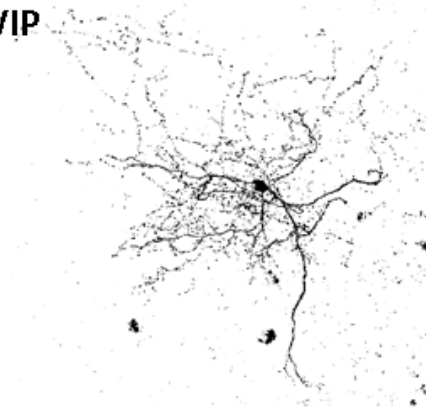
Figure 6. Images of representative cell types, firing patterns and responses of cells in the BA that have been examined the effects of cholinergic inputs originating from the BF. Blue light stimulation (5 ms, 2 mW LED) of ChR2 was delivered with 10 Hz. Lower: summary graph of the results.

As comparison, we also examined the properties of PV+ projection of the BF to the BA. We injected AAV2/5-DIO-ChR2-eYFP or AAV2/5-DIO-ChR2-mCherry to the BF and after 3-4 weeks of expression we prepared acute brain slices to investigate light-evoked synaptic currents in BA cell types (Figure 7).
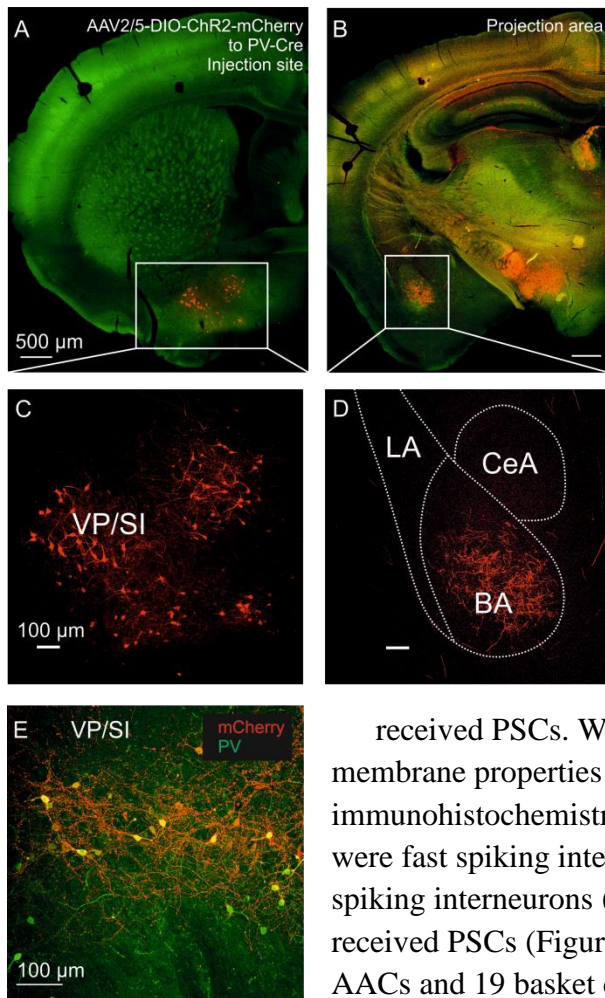
Figure 7. Injection site (A, C) in the BF of a PV-Cre mouse and axonal projection in the BA (B, D) in red. In images taken at lower magnification, autofluorescence background was taken in green channel for better visualization of the structures in a coronal plane of the samples. E: Staining of viral construct-labeled cells in the BF for PV revealed high overlap of the two markers verifying the proper functioning of the Cre-lox system in the experiments.

In this case we targeted somata in slices containing the BA that were surrounded by fluorescent-protein expressing terminals. Out of 346 cells tested (183 were interneurons and 163 were principal cells) in the BA, we found light-evoked PSCs in one-third (29%) of recorded neurons. We found a preference for innervation onto interneurons, as 39% of interneurons (71 out of 183) and only 18% of PCs (30 out of 163) received PSCs. We identified the cell types based on intrinsic membrane properties and morphology revealed with immunohistochemistry after recordings. Among interneurons, 45% were fast spiking interneurons (37 out of 82), 38% were regular spiking interneurons (13 out of 34) and 15% were NGFCs that received PSCs (Figure 8). Among fast spiker cells, we identified 20 AACs and 19 basket cells (BCs) based on fact whether the axon of the investigated interneuron formed close appositions with the axon initial segments labeled by ankyrin-G (typical for AACs) or the soma of the tested interneuron contained calbindin (typical for BCs) using immunocytochemistry. We found no differences between these two fast spiker cell types either in probability or amplitude of PSCs.
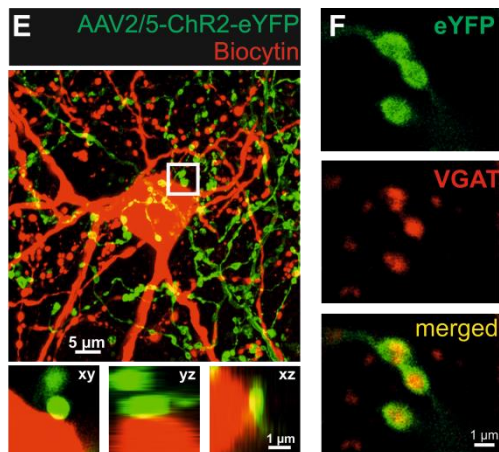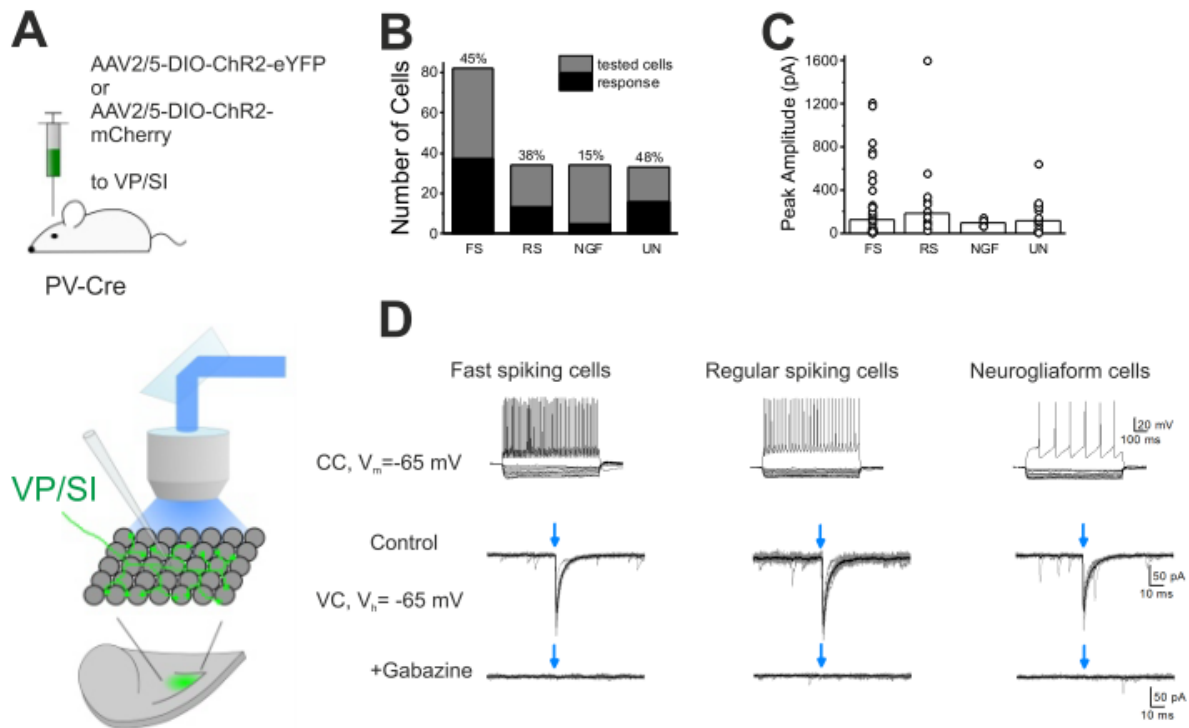
Figure 8. Light-evoked IPSCs could be detected in several types of interneurons in the BA by local stimulation of PV-expressing BF axons. A, Scheme of *in vitro* experiments, B, Number of tested interneuron types and ratio of the detected synaptic responses. FS: Fast spiking interneurons, RS: Regular spiking interneurons, NGF: Neurogliaform cells, UN: Unidentified interneurons. C, Amplitude of IPSCs in the four categories of interneurons. D, Example of firing pattern of cells and synaptic responses. IPSCs could be abolished by gabazine (2 µm) in all cases tested indicating that GABA-A receptors mediate the postsynaptic responses. Blue light illumination (2 ms, 2 mW) is indicated with blue arrow. E, Confocal image of a recorded interneuron visualized *post-hoc* due to the filling of biocytin (Cy3 SA, red) and the surrounding axons from the BF (eYFP, green). Higher magnification of a synaptic contact shown in three 3D directions. F, VGAT-staining revealed that the PV boutons from the BF indeed contain GABA transporter, a necessary component for releasing GABA from vesicles.

Additionally, we also investigated how this inhibition deriving from the BF can influence the firing of target cells. To this aim, we locally puffed glutamate (0.5 mM) close to soma of cells to evoke firing while activated ChR2-expressing BF terminals with blue light. We recorded first the firing of cells in loose patch mode, and then performed recordings in voltage clamp mode from the same cells to reveal the features of light-evoked PSCs. We found that in those cells, which received PSCs with amplitude of at least 100 pA, the glutamate-evoked firing could be blocked by activation of BF input (Figure 9). The results of this study was presented at the FENS 2016 in held Copenhagen titled "GABAergic input from the basal forebrain controls fear generalization by regulating GABAergic interneurons in the mouse basolateral amygdala".
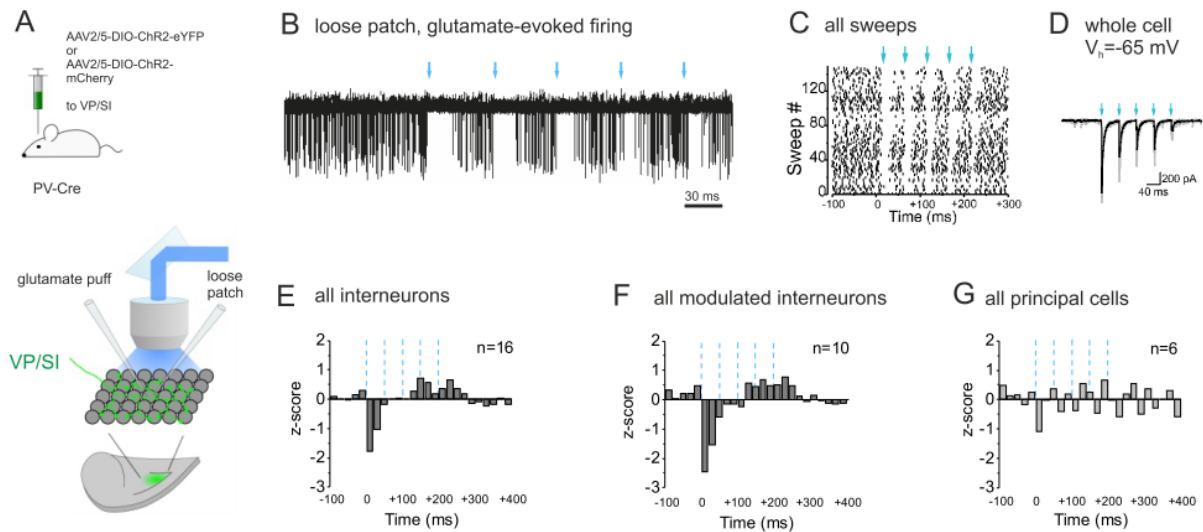
Figure 9. The firing of the interneurons but not the principal cells in the BA could be effectively modulated by the GABAergic input from the basal forebrain. A, Schematic drawing of loose-patch experiments. B, Raw traces of a representative cell, multiple sweeps were superposed. C, Raster plot of firing obtained for the same cell shown in B. D, Synaptic currents were revealed after loose patch experiments in voltage clamp mode by re-patching the same cell. E-G, z-score plot of firing in interneurons and principal cells, time points of blue light stimulation are indicated with dashed lines.

In the final part of the project, we continued to examine the role of BF cholinergic and GABAergic afferents in aversive learning. To this end, we established Pavlovian fear conditioning combined with optogenetics in the laboratory. We tested whether inhibition of BF fibers in the BA can affect learning if applied during delivery of aversive stimuli. First, we tested the effect of inhibition of all types of fibers by expressing ArchT inhibitory opsin under the control of CAG promoter in BF cells. After behaviour testing, we found that inhibition of BF projection fibers in the BA tended to decrease the efficiency of conditioned learning. As this effect was not significant, we went on with promoter specific expression of ArchT to selectively test for the effect of GABAergic, cholinergic, and parvalbumin-expressing GABAergic projection in conditioned learning. Therefore, we used VGAT-Cre, ChAT-Cre and PV-Cre mouse lines, and expressed AAV2/8-Flex-ArchT-GFP or AAV2/8-Flex-GFP as control in the BF cells. So far, our results are contradictory. Inhibition of VGAT-positive input had a tendency to increase, but inhibition of ChAT- and PV-positive input had a tendency to decrease the efficiency of fear learning (Figure 10). None of the observed differences were significant, though we were aiming to test for a different approach to clarify the role of BF projection to the BA in aversive learning.
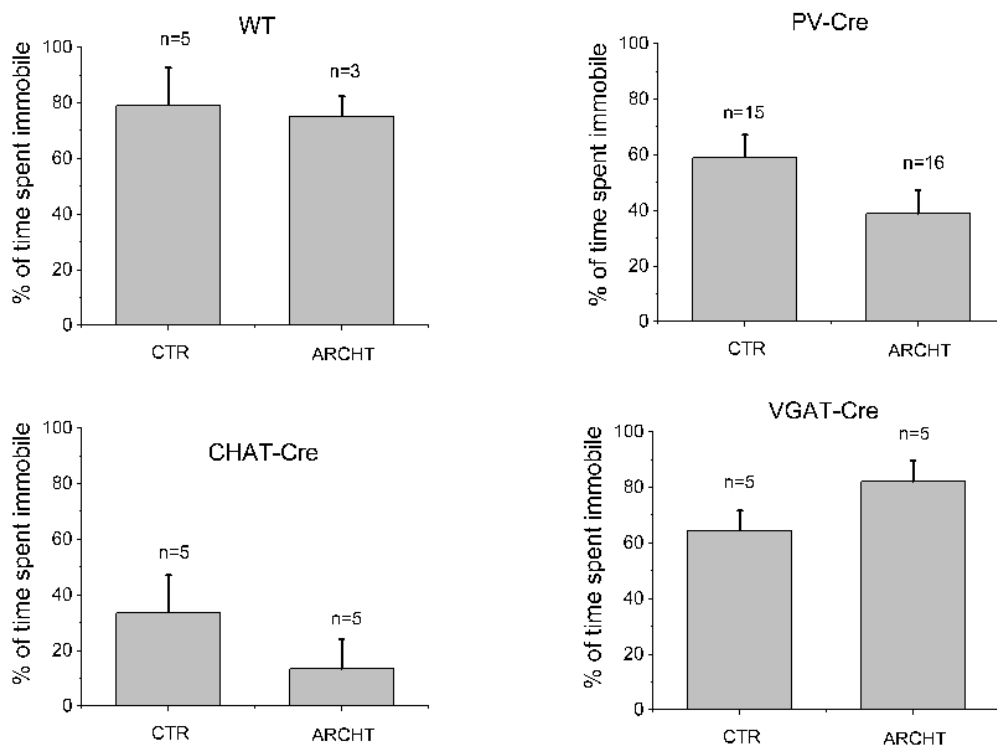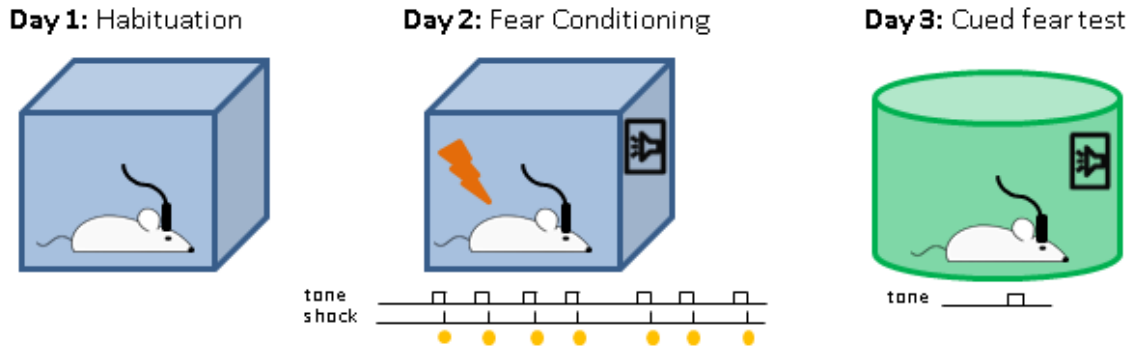
Figure 10. Schematic picture of the fear conditioning protocol (upper part) and graphs (lower part) showing the effect ArchT-mediated inhibition of BF fibers in WT, PV-Cre, CHAT-Cre and VGAT-Cre animals during aversive stimuli on immobility upon the first sound on the testing day.

We established local drug application to the BA with cannula, and we performed inhibition of axonal projections from the BF during fear conditioning using the inhibitory DREADD-system. So far, we injected AAV2/8-DIO-HM4D-mCherry viral vector and AAV2/8-DIO-mCherry control construct to two groups of PV-Cre mice and injected the DREADD agonist CNO (20 µM, 200 nl) locally to the BA 30 minutes before fear conditioning. In this experiment, we found that the efficacy of learning decreased in mice where the DREADD was expressed in BF fibers (Figure 11). Therefore, we can conclude that BF PV cells have a role in conveying information related to aversive stimuli to the BF during associative

learning. We are aiming to test the other (VGAT+, CHAT+) projections as well to compare the different pathways.
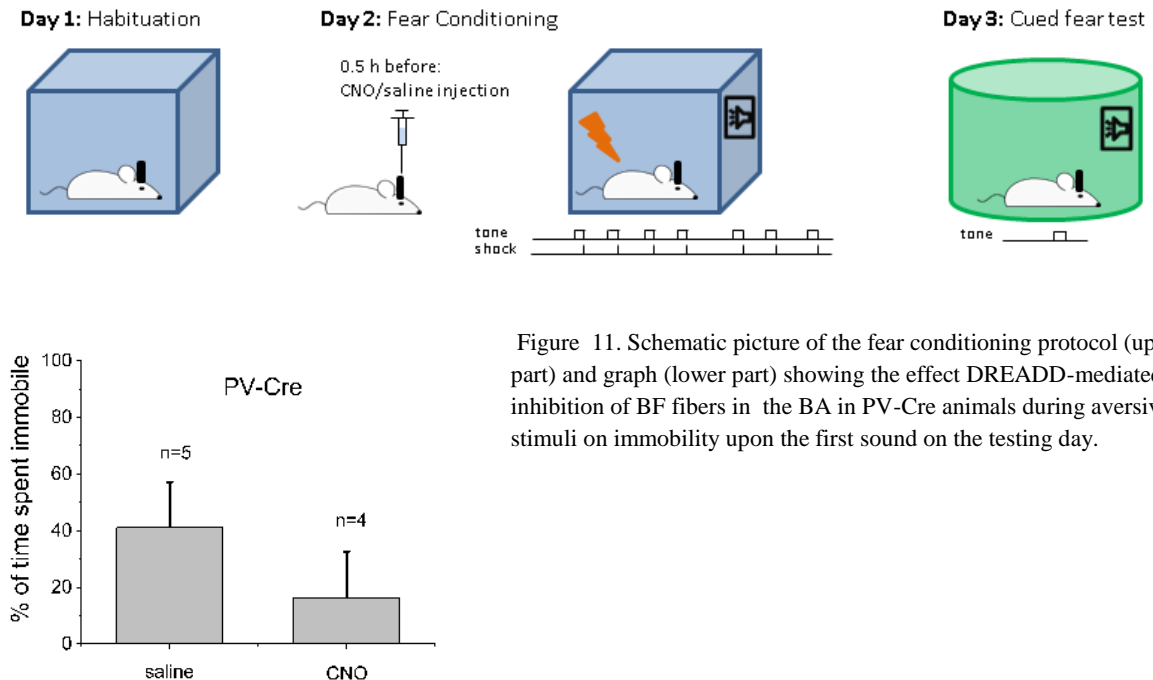
Figure 11. Schematic picture of the fear conditioning protocol (upper part) and graph (lower part) showing the effect DREADD-mediated inhibition of BF fibers in the BA in PV-Cre animals during aversive stimuli on immobility upon the first sound on the testing day.

The verification of the latter experiments is still ongoing. We haven't published articles from the data presented here, but we foresee publishing 2 or 3 articles from these results within the next two years. For this reason, I'm going to ask for re-evaluation of the grant outcomes upon publishing the papers related to the topic of my PD grant.

References

Courtin J, Bienvenu TC, Einarsson EO, Herry C (2013) Medial prefrontal cortex neuronal circuits in fear behavior. Neuroscience 240:219-242.

Craig LA, Hong NS, Kopp J, McDonald RJ (2009) Cholinergic depletion of the medial septum followed by phase shifting does not impair memory or rest-activity rhythms measured under standard light/dark conditions in rats. Brain Res Bull 79:53-62.

Duvarci S, Paré D (2014) Amygdala microcircuits controlling learned fear. Neuron 82:966-980.

Hangya B., Ranade S. P., Lorenc M., Kepecs A. (2015) Central cholinergic neurons are rapidly recruited by reinforcement feedback. Cell 162 1155–1168. 10.1016/j.cell.2015.07.057

Jiang L, Kundu S, Lederman JD, López-Hernández G, Ballinger E., Wang S, Talmage DA, Role LW (2016) Cholinergic Signaling Controls Conditioned Fear Behaviors and Enhances Plasticity of Cortical-Amygdala Circuits. Neuron. 90, 5.: 1057–1070.

Kaifosh P, Lovett-Barron M, Turi GF, Reardon TR, Losonczy A (2013) Septo-hippocampal GABAergic signaling across multiple modalities in awake mice. Nat Neurosci 16:1182-1184.

Kim J, Pignatelli M, Xu S, Itohara S Tonegawa S (2016) Antagonistic negative and positive neurons of the basolateral amygdala. Nature Neuroscience. 19, 12.: 1636–1646.

Pape HC, Paré D (2010) Plastic synaptic networks of the amygdala for the acquisition, expression, and extinction of conditioned fear. Physiol Rev 90:419-463.

Poulin AN, Guerci A, Mestikawy SE, Semba K (2006): Vesicular Glutamate Transporter 3 Immunoreactivity Is Present in Cholinergic Basal Forebrain Neurons Projecting to the Basolateral Amygdala in Rat. The Journal Of Comparative Neurology. 498, 5. 690–711

Senn V, Wolff SB, Herry C, Grenier F, Ehrlich I, Gründemann J, Fadok JP., Müller C, Letzkus JJ., Lüthi A (2014) Long-range connectivity defines behavioral specificity of amygdala neurons. Neuron. 81, 2.: 428–437.

Tronson NC, Schrick C, Guzman YF, Huh KH, Srivastava DP, Penzes P, Guedea AL, Gao C, Radulovic J (2009) Segregated populations of hippocampal principal CA1 neurons mediating conditioning and extinction of contextual fear. J Neurosci 29:3387-3394.